UWB Horn Antenna for Food Inspection via Microwave Imaging

J. F. González-Pardo*(1), C. I. Maraloiu(1), J. A. Tobón Vasquez(2), M. Ricci(2) and F. Vipiana(1)
(1) Politecnico di Torino, Torino, Italy, francesca.vipiana@polito.it
(2) Wavision s.r.l., Torino, Italy, marco.ricci@wavision.it

Abstract

This paper presents the design and the numerical modelling of an ultra-wideband Extended Gap Ridged Slotted Horn (EGRSH) antenna for food inspection via microwave imaging. By integrating slots and a low-permittivity filler material, the antenna extends its operation range from 3 up to 11 GHz, while maintaining a compact size. The design is validated for detecting low-density contaminants like Polytetrafluoroethylene (PTFE), within oil-based foods packaged in glass containers. A dielectric contrast map, computed with the Truncated Singular Value Decomposition (TSVD) method under Born approximation, results in a successful estimation of the contaminant position.

1 Introduction

Foreign body contamination is one of the main factors that can make a product unappealing to consumers, leading to reputational damage for the manufacturer and a decline in sales. To mitigate this problem, a wide range of food inspection and safety systems are available nowadays, including metal detectors and X-ray imaging systems to name a few. However, these technologies face problems when detecting non-metallic and low-density contaminants. This is particularly critical because these materials can be used in food packaging, such as plastics and glass [1]. To address these limitations, microwave-based systems have emerged as an alternative, as they are sensitive to changes in the dielectric properties of an object under test, producing measurable variations.

Microwave imaging (MWI) systems have been studied in the last years for applications in the food industry [2, 3]. Their operating principle is based on the estimation of dielectric contrast, where small perturbations, such as the presence of contaminants, result in variations in the total electromagnetic field. These changes can be measured by comparing the scattering parameters in the presence and absence of a contaminant. A critical challenge in these systems is the design of the radiating element, as it typically requires broadband antennas with low cut-off frequencies around 1 GHz to ensure sufficient penetration into the object under test, and high frequencies to enhance resolution. Monopole antennas have been widely used for this purpose in both industrial [2] and biomedical applications [4],

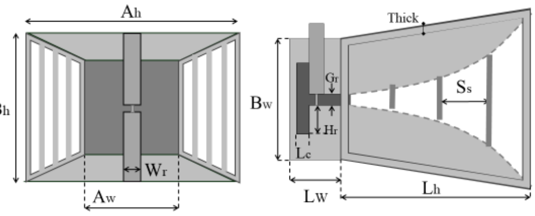

Figure 1. Designed Extended Gap Ridge Slotted Horn antenna (EGRS).

primarily due to their simpler fabrication and broad bandwidth. However, their radiated field is unfocused, leading to poor illumination within the imaging domain and reducing the quality of the resulting MWI. To address this limitation, [5] proposed a horn antenna capable of focusing the radiated field. However, this design significantly reduces bandwidth, making it unsuitable for microwave imaging applications.

In this work, we present the design of an ultra-wide band Extended Gap Ridged Slotted Horn (EGRSH) antenna for microwave imaging applications. The integration of slots in the horn's ground plane, combined with the inclusion of a low-permittivity, low-loss filler material inside its cavity, allowed the extension of the operation range from 3 up to 11 GHz. Despite its broad bandwidth, and a low cut-off frequency, the antenna maintains a compact size of $43 \times 40 \times 41$ mm, making it suitable for food inspection.

2 Antenna Desing

The proposed design is inspired by the antenna in [5], developed for biomedical applications. The horn consists of waveguide-feeding and ridge-horn transition sections, fed with a coaxial line which enter from the upper ridge, and short-circuited with the lower ridge, achieving an operating range from 0.5 to 3 GHz in biomedical applications. Nevertheless, this frequency range is inadequate for food inspection, mainly due to the small size of typical contaminants. To address this limitation, the upper cutoff frequency should be increased to enhance the resolution, but maintaining a lower cutoff frequency, which ensures deeper penetration of a microwave imaging system. According to the requirements, slots are integrated into the horn to increase bandwidth and improve coupling at high frequencies. Ad-

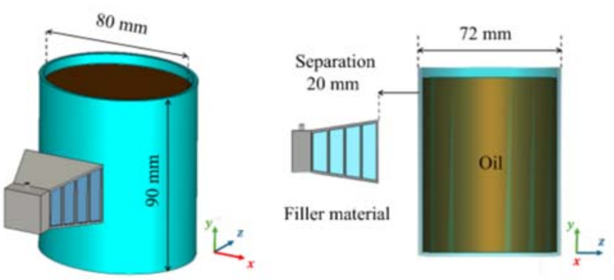

Figure 2. Simulated scenario with a glass jars filled with oil.

ditionally, a filler material is introduced inside the cavity to lower the cutoff frequency [6], without affecting the size of the antenna. Figure 1 shows the geometry of the proposed EGRSH antenna, whose dimensions are optimized by simulating a scenario for detecting non-metallic solid contaminants within oil ($\varepsilon_r = 2.9$ and $\sigma = 0.21$ S/m at 10 GHz [2]) packaged in glass jars (see Fig. 2). All the geometrical dimensions of the optimized antenna are reported in Table 1, and the dielectric material is Ecoflex™ 00-30, with $\varepsilon_r = 2.95$ and $\sigma = 0.17$ S/m at 10 GHz). The proposed antenna is compared with the one proposed in [5], considering the scenario in Fig. 2. As shown in Fig. 3, the magnitude of the reflection coefficient of the proposed is lower than -10 dB from 4 GHz, significantly increasing the bandwidth of [5].

Figure 4 shows the electric field distribution inside the oil-filled jar under test, across two xy-plane slices at z = 75 mm and z = 95 mm (middle of the jar), at frequencies of 2, 3, 4, 9, 10, and 11 GHz. As expected, the footprint size decreases with increasing frequency, as the penetration depth. Additionally, losses from the filler material and the oil contribute to a reduction in field magnitude, representing a 4 dB loss with respect to the maximum field observed at 3 GHz. Nevertheless, from 3 GHz, power is effectively concentrated around the aperture plane projected onto the simulated slices.

Table 1. Dimensions of proposed antenna

Name	[mm]	Name	[mm]	Name	[mm]
Ah	43	Bh	30	Lh	3
Aw	20	Bw	20	Lw	9
Wr	3.3	Hr	5.04	Lc	3.5
Gr	1.4	Ss	7.625	Thick	1

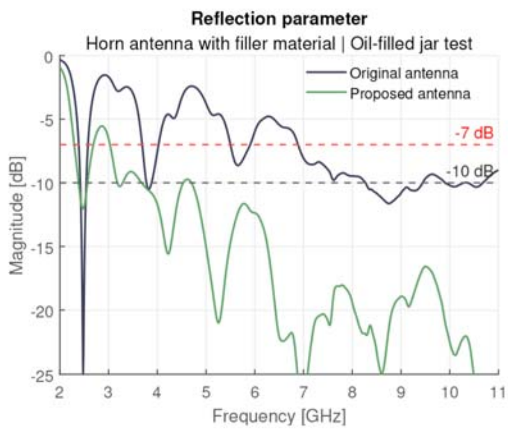

Figure 3. Reflection coefficient of the EGRHS antenna in front of oil-filled jar.

3 MWI System Design

In industrial production lines, packaged food is transported throughout the plant on extensive conveyor belts. Consequently, MWI systems must be designed so that it can be integrated correctly, without affecting production. This requires balancing the restrictions in spatial distribution of the antennas (limiting the sensors) with the illumination inside the object under test. First, the bottom of the target is restricted by the conveyor line, leaving only the top and sides available for antenna placement. Second, the average field distribution inside the jar must ensure proper illumination while minimizing low-field regions. Accordingly, a total of six EGRSH antennas are placed, arranged in a 3-3 distribution on each side of the conveyor belt, directing the aperture to the oil-filled glass jar, as shown in Fig. 5.

In the presence of a radiated field produced by a transmitting antenna, the contaminant induces a variation in the measured scattering parameters. Given a small perturbation in the field distribution, i.e. the contaminant size is much smaller than the wavelength, the Born approximation can be applied. This method assumes that the total field $\mathbf{E^t}$ (the sum of the scattered field $\mathbf{E^s}$ and the incident field $\mathbf{E^i}$, i.e. without contaminant) is approximately to the incident field. Consequently, the scattered field at $\mathbf{r}_n$, due to the field radiated by a source in $\mathbf{r}_m$, can be expressed as [7, 8]:

$$E^s(r_n, r_m) = i\omega\mu_0 \iiint_D \mathbf{E}^i(\mathbf{r}, \mathbf{r}_m) \cdot \mathbf{E}^i(\mathbf{r}, \mathbf{r}_n)\chi_e(\mathbf{r})\, d\mathbf{r} \quad (1)$$

where D is the image domain, ω is the angular frequency, i is the imaginary unit, μ_0 is the vacuum permeability, $\mathbf{r}_m$ and $\mathbf{r}_n$ is the position of the transmitting and receiving antennas. To apply this model, the integral of the equation must be discretized by evaluating the field within the domain of interest (inside the jar). This is computed by full-wave simulation of the proposed scenario, from which the spatial distribution of incident electric field (without contaminant) and the scattering parameter matrix are extracted. In this way, the behavior of the difference of the scattered parameters (ΔS) with and without contaminant can be linearized as it is related with the dielectric contrast by the expression:

$$[\Delta S] = [\mathscr{L}][\Delta\chi_e] \qquad \text{for} \quad \Delta\chi_e = \frac{\varepsilon_c - \varepsilon_b}{\varepsilon_b} \quad (2)$$

where $\Delta\chi_e$ is the dielectric contrast, ε_c is the complex permittivity of the contaminant and ε_b is the complex permittivity of the surrounding medium (oil). The matrix $[\mathscr{L}]$ has

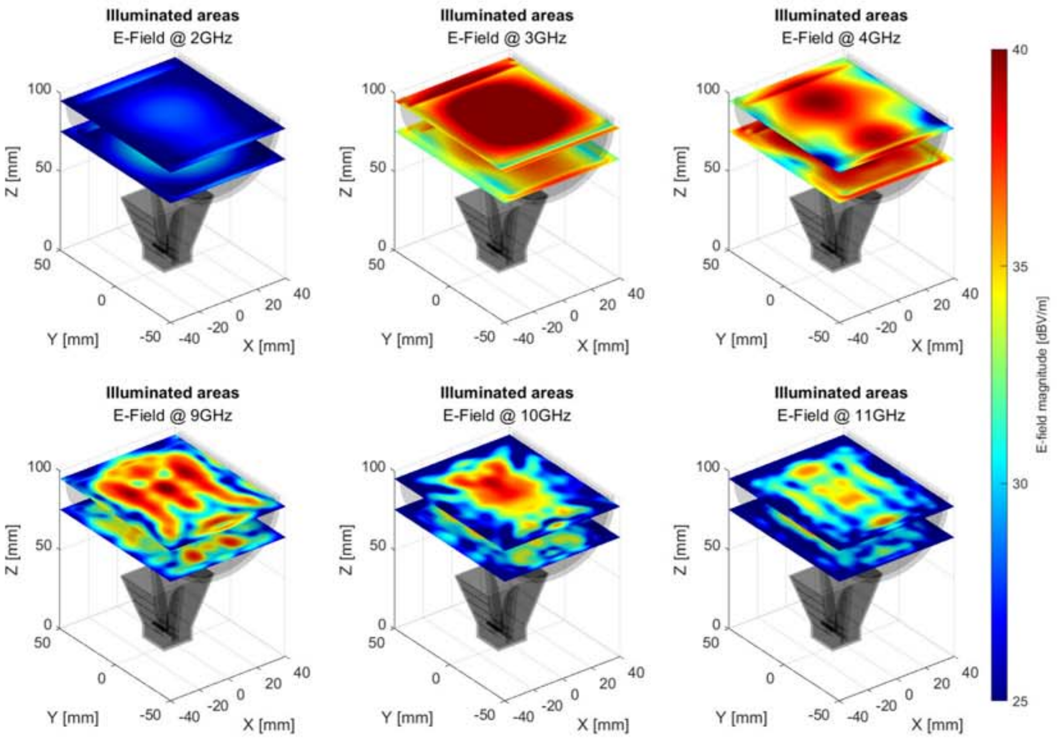

Figure 4. Electric field distribution inside the oil-filled jar.

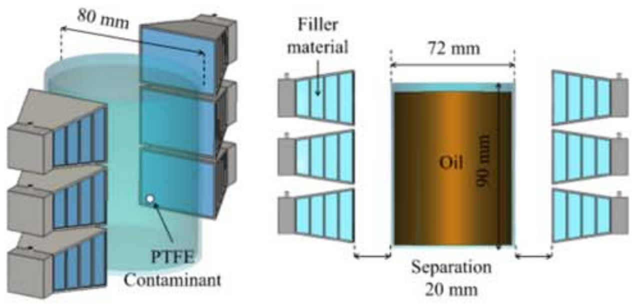

Figure 5. Antenna array configuration for MWI in food inspection. As contaminant a PTFE sphere of 2 mm radius inside the jar.

dimensions $N_c \times (N_{tx} \cdot N_{rx})$, where N_c is the number of field samples within the image domain, N_{tx} and N_{rx} the number of transmitting and receiving antennas, respectively. Each column of this operator is computed by the product of all possible incident field combinations within the domain D. A well-known method to face the equation (2) is the truncation of the singular value decomposition of the matrix $[\mathscr{L}]$ (TSVD) [9]. Let $[\mathscr{L}] = [U][\Sigma][V]$, $\Delta\chi_e$ could be computed as:

$$\Delta\chi_e = \sum_{n=1}^{T} \frac{1}{\sigma_n} \langle [\Delta S], [u_n] \rangle [v_n] \tag{3}$$

Where σ_n corresponds to the nth singular value, and singular left and right vectors of $[\mathscr{L}]$, respectively. While T represents the truncation index, which for this case is defined as the point where the magnitude of the nth normalized eigenvalue is less than -20 dB.

We consider the scenario in Fig. 5, and compute $\Delta\chi_e$ at 3, 4, 9, 10 and 11 GHz using (3). As contaminant a PTFE sphere of 2 mm radius is placed in (15, -15, 95) along the x, y and z axis, respectively. We consider a critical scenario, not only for the contaminant material, which is not detected with available systems [1], but for the low dielectric contrast with respect to the background material (oil). As observed before, the EGRSH antenna produces a more uniform field distribution along its operation range, give us a good reconstruction of the image using multi-frequency information. Fig . 6 shows the reconstructed normalized dielectric contrast within the oil-filled jar caused by the PTFE contaminant. This image is generated by multiplying the dielectric contrast at each simulated frequency and then normalizing it by its maximum value. From left to the right, cut planes were constructed to visualize the predicted contaminant position using this method. As observed, the highest contrast generally corresponds to the expected position of the contaminant, but its shape is distorted. This distortion is mainly due to the acquisition geometry and can be eliminated by increasing the number of sample points, i.e changing the jar position to simulate the movement of the conveyor belt [3] or using the Illumination Balancing algorithm (IBA), [2].

4 Conclusion and Perspectives

This work presented the design and numerical validation of an ultra-wideband Extended Gap Ridged Slotted Horn antenna for microwave imaging applications. Techniques such as the inclusion of horn slots and the integration of a

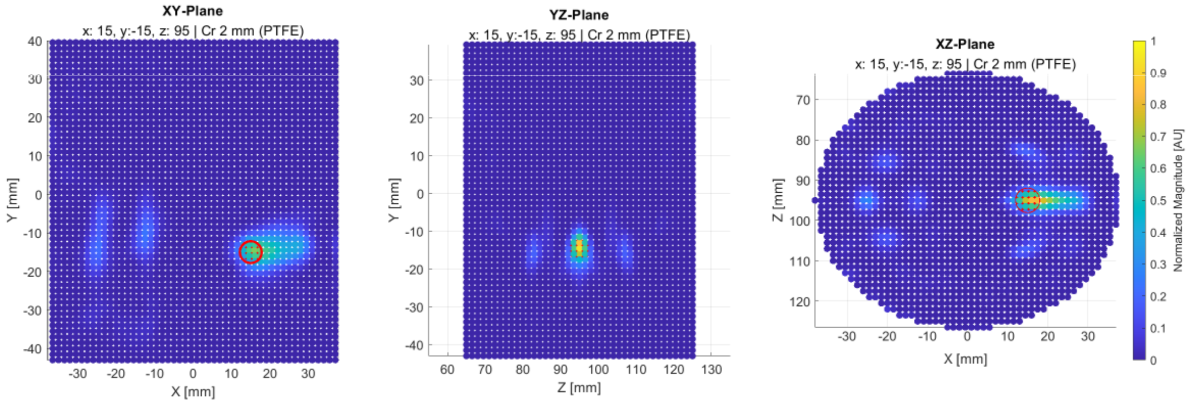

Figure 6. Normalized dielectric constant maps constructed by multiplying the contrast computed at each simulated frequency, obtained inserting a 2 mm radius PTFE contaminant located in the position (15, -15, 95). (a) xy-plane cut with z = 95 mm, (b) zy-plane, with x = 15 mm and (c) xz-Plane with y = -15 mm.

low-permittivity, low-loss filler material allowed for an extended operational bandwidth while maintaining a compact size. Additionally, the design was evaluated by constructing the dielectric contrast map using the TSVD method as a solution to the Born approximation. An acquisition system consisting of six antennas positioned along the sides of the conveyor belt is proposed. The results demonstrated that the contaminant induces an observable perturbation in the contrast dielectric image, with maximum values aligning with its theoretical position. However, the contaminant size is affected by the acquisition geometry, an issue that could be improved by increasing the number of measurements and varying the jar's position or using the balancing illumination algorithm [2].

As future work, we propose validating this design for other types of contaminants with also different food products. Additionally, we propose to consider the movement of the production line in order to observe its effects on the image reconstruction process.

5 Acknowledgements

This work is supported in part by “INSIGHT-FOOD, An innovative microwave sensing system for the evaluation and monitoring of food quality and safety”, funded by MAECI, in part by PNRR-NGEU (DM117/23), in part by PON Research and Innovation "Microwave Imaging and Detection powered by Artificial Intelligence for Medical and Industrial Applications" (DM1062/21), and in part by PRIN "BEST-Food, Broadband Electromagnetic Sensing Technologies for Food Quality and Security Assessment”, all funded by MUR.

References

[1] TDI Packsys, “X-ray food inspection processes and capabilities,” https://www.tdipacksys.com/blog/x-ray-food-inspection-processes-and-capabilities/, 2023.

[2] M. Ricci, J. A. T. Vasquez, R. Scapaticci, L. Crocco, and F. Vipiana, “Multi-antenna system for in-line food imaging at microwave frequencies,” *IEEE Transactions on Antennas and Propagation*, vol. 70, no. 8, pp. 7094–7105, 2022.

[3] J. A. Tobon Vasquez, R. Scapaticci, G. Turvani, M. Ricci, L. Farina, A. Litman, M. R. Casu, L. Crocco, and F. Vipiana, “Noninvasive inline food inspection via microwave imaging technology: An application example in the food industry,” *IEEE Antennas and Propagation Magazine*, vol. 62, no. 5, pp. 18–32, 2020.

[4] S. Ullah, C. Ruan, M. S. Sadiq, T. U. Haq, and W. He, “High efficient and ultra wide band monopole antenna for microwave imaging and communication applications,” *Sensors*, vol. 20, no. 1, 2020.

[5] S. Rashid, L. Jofre, A. Garrido, G. Gonzalez, Y. Ding, A. Aguasca, J. O'Callaghan, and J. Romeu, “3-D Printed UWB Microwave Bodyscope for Biomedical Measurements,” *IEEE Antennas and Wireless Propagation Letters*, vol. 18, no. 4, pp. 626–630, 2019.

[6] D. M. Pozar, *Microwave engineering: theory and techniques*. John wiley & sons, 2021.

[7] N. K. Nikolova, *Introduction to Microwave Imaging*. Cambridge University Press, 2017.

[8] X. Chen, *Computational Methods for Electromagnetic Inverse Scattering*. JohnWiley & Sons Singapore Pte. Ltd, 2018.

[9] M. Bertero, P. Boccacci, and C. De Mol, *Introduction to inverse problems in imaging*. CRC press, 2021.